Environment International 146 (2021) 106177

Contents lists available at ScienceDirect

Environment International

journal homepage: www.elsevier.com/locate/envint

Developing a UV climatology for public health purposes using satellite data

Laurent Vuilleumier [a,*], Todd Harris [b], Athanasios Nenes [b,c], Claudine Backes [d], David Vernez [d]

[a] Federal Office of Meteorology and Climatology (MeteoSwiss), Payerne, Switzerland
[b] Laboratory of Atmospheric Processes and their Impacts, School of Architecture, Civil and Environmental Engineering, Swiss Institute of Technology, Lausanne, Switzerland
[c] Institute of Chemical Engineering Sciences, Foundation for Research and Technology Hellas, Patras, Greece
[d] Center for Public Health and Primary Care Medicine (Unisanté), University of Lausanne, Switzerland

ARTICLE INFO

Handling Editor: Xavier Querol

Keywords:
Ultraviolet
Climatology
Satellite imagery
Public health
Environmental health
Skin cancer

ABSTRACT

The effects of solar ultraviolet (UV) radiation on life on Earth differ greatly. While overexposure to UV rays is harmful, small amounts of exposure are necessary for the synthesis of Vitamin D and good health. To optimize individual exposure to solar UV, it is therefore crucial to use UV data sources representative for entire populations and realistically accounting for various influencing factors. A UV climatology for Switzerland based on satellite data has been developed to provide risk estimates at population level. An algorithm generating ground-based radiation estimate has been transformed from the visible to the UV wavelength domain by adapting both a clear-sky radiation transfer model and a cloud modification factor model using satellite imagery.

The algorithm allows the computation of global UV erythemal irradiance at a spatial resolution of 1.5 – 2 km and an hourly temporal resolution over fifteen years. A validation, conducted with measurements from three meteorological stations over ten years, showed that the expanded uncertainty for low hourly UVI values (UVI $<$ 3) is about $\pm$ 0.3, while for high hourly UVI values (UVI $>$ 6) it can go up to $\pm$ 1.5. In clear-sky situation, the uncertainty is in the range of 10–15%.

The climatology developed allows to visualise potential UV exposure at regional and national scale. National prevention intervention could use new strategies to better focus on populations at risk and better tailor available researches. The UV climatology allows a high versatility in adapting the data extraction to the goal of studies using it. Further tailored data extraction and analysis will be necessary to exploit this climatology in a wide range of environmental and occupational health applications. Its development was focused on Switzerland, but the techniques used can be extended globally.

1. Introduction

1.1. The need for higher quality UV data at population level

Solar Ultraviolet (UV) radiation is an important determinant of environmental and occupational health. UV radiation exposure induces cellular stress through the generation of reactive oxygen species that can damage cells, leading to adverse health outcomes as skin cancer, cataracts, sunburn, skin ageing and immunosuppression (Armstrong and Kricker 2001). Considering nine diseases associated to UV exposure, the World Health Organisation (WHO) estimated that excessive solar UV exposure caused yearly the loss of approximately 1.5 million DALYs (disability-adjusted life years) worldwide and 60 000 premature deaths (Lucas et al. 2008). However, the relationship between health effects (such as various skin cancers) and exposure patterns is not yet well understood. Cutaneous malignant melanoma (CMM) is associated mostly with acute exposure (sunburns), squamous cell carcinoma (SCC) with chronic exposures and basal cell carcinoma (BCC) is generally associated with both intermittent and chronic exposures. Thus defining "excessive exposure" is not a simple matter.

Interestingly, solar UV exposure is also associated with indirect, health promoting effects as the natural production of vitamin D by UV radiation in exposed skin zones (Deluca 2014). Sufficient vitamin D doses are essential for skeletal health, have a preventive effect on some respiratory tract infections and autoimmune diseases (Cantorna, 2006; Martineau et al., 2019). Ideally, solar UVR exposure must be balanced to avoid the adverse health effects associated with insufficient or excessive

* Corresponding author at: Federal Office of Meteorology and Climatology MeteoSwiss, Ch. de l'Aérologie 1, 1530 Payerne, Switzerland.
E-mail addresses: laurent.vuilleumier@meteoswiss.ch (L. Vuilleumier), todd.harris@epfl.ch (T. Harris), athanasios.nenes@epfl.ch (A. Nenes), claudine.backes@unisante.ch (C. Backes), david.vernez@unisante.ch (D. Vernez).

https://doi.org/10.1016/j.envint.2020.106177
Received 26 February 2020; Received in revised form 30 September 2020; Accepted 30 September 2020
Available online 12 November 2020

Abbreviations

BCC	Basal Cell Carcinoma
ER	Exposure Ratio
MM	Cutaneous Malignant Melanoma
SCC	Squamous Cell Carcinoma
SZA	Solar Zenith Angle
SED	Standard Erythemal Dose
UVA/UVB	Specific UV bands
UVI	UV Index

exposure (Religi et al. 2019).

The UV Index (UVI) scale from the WHO condenses the spectrum of UV radiation intensity into a single number according to the *erythemal* action spectrum – the relative importance of different UV wavelengths in causing sunburn. The WHO promotes simple messages advising the public on the recommended level of exposure prevention (such as hats and sunscreen) according to the UVI value. This international standard measure has recently faced criticism for its lack of usability in various geographical locations and for poor preventive recommendations at low UV intensity levels (Gies et al. 2018).

For epidemiological studies, common methods for the tabulation of UV exposure involve survey studies combined with personal measurements from wearable dosimeters (Moldovan et al. 2019). However, this method can be costly and overly specific with new research often requiring a new dosimetry campaign. A more general approach is to use ambient UV irradiance, readily available from several datasets, and assume it to be proportional to the total daily UV dose – the cumulative UV exposure over 24 h. Globally, ambient UV irradiance is influenced by environmental factors resulting in high spatial and temporal variability, as the solar zenith angle (SZA) depending on location and time of year, cloudiness, altitude, and the ozone concentration in the atmosphere. Individual factors significantly influence the effective UV dose, including the day time spent outdoors, the use of sun protective means (clothes, sunglasses, sunscreen), and the level of shade-seeking behaviour.

Effective Dose (ED) can be deduced from ground irradiance, over time of exposure, using the Exposure Ratio (ER), which is defined as the fraction of the surrounding radiation received by an individual or on a particular anatomical area relative to a horizontal surface. ER is used as corrective factor, emulating the exposure attenuation brought by local and behavioural factors (Vernez et al. 2015).

There are two primary sources of ambient irradiance data, in situ measurements and remote sensing via satellite. In situ measurements using spectroradiometers (Bernhard and Seckmeyer 1999) or broadband radiometers (Hulsen and Grobner, 2007; Milon et al., 2014; Vernez et al., 2011) provide the most precise determination of local radiation intensity. However, these measurements are spatially sparse (for example in Switzerland only four stations have been measuring UV over the long-term), which significantly restricts their generalization. Alternatively, combining satellite measurements with Radiative Transfer Models (RTMs) can produce UV datasets that are continuously extended over space and time, a key advantage over both in situ and dosimetry measurements. In adopting a public health, population-based vision of risk, high spatial resolution and extension are important for comparisons with population distributions, thus satellite-based UV data has excellent epidemiological applications. However, for the estimation of potential risk as defined above we require particularly high quality data for which existing satellite-based UV datasets may not be satisfactory.

1.2. Satellite-based UV data

To answer the needs of public health or epidemiology studies, high quality UV data must have kilometre-scale spatial resolution (to account for altitude changes in mountainous area), hour-scale temporal resolution (to account for changes in ER throughout the day), and accurately consider the moderating role of meteorological effects on UV radiation. Furthermore, this data must be extended over many years to determine long-term average exposures (i.e. chronic exposure linked to BCC and SCC) and probabilities of extreme exposure events (i.e. acute exposure linked to CMM). Currently available UV datasets do not cover all of these aspects. Here we review four such datasets. First, a European dataset of reconstructed UV irradiance was produced by COST Action 726 (Koepke et al. 2006). Second, the Tropospheric Emission Monitoring Internet Service (TEMIS) that uses observations from nadir-viewing satellite instruments such as GOME, SCIAMACHY (van Weele et al. 2005). Third, we note that some UV subsets have been developed as part of global solar datasets like the Solar radiation Data (SoDa) Service as part of the EuroSun project. Fourth, we consider a project investigating the effects of radon and UV exposure on skin cancer mortality that developed a climatology of UV radiation in Switzerland (Vienneau et al. 2017).

- The dataset produced by COST Action 726 has a spatial extent covering all Europe (from 25.5° W to 35.5° E and 30.5 to 80.5° N) at a spatial resolution of 0.05° or 4 to 5 km depending on the latitude. It covers an extended temporal period (01–01-1958 to 31–08-2002) at a daily temporal resolution. It is based on a UV reconstruction technique (Koepke et al. 2006) and thus relies on input data that can be affected by significant uncertainties. In particular, the information used for inferring the effect of clouds on UV irradiance is derived from the ERA-40 reanalysis from the European Centre for Medium-Range Weather Forecasts (ECMWF) interpolated on a 1° grid. This is much coarser than the 0.05° output grid and thus leads to considerable imprecision in the dataset.
- TEMIS is a global service primarily oriented toward forecasts. Archived forecasts are available worldwide, but only for *clear-sky* UV estimates (the cloud effect is not accounted for). Cloud-modified total UV dose data are available at a daily temporal resolution. The data used for inferring the cloud effect are obtained from Meteosat Second Generation (MSG) satellite observations. The spatial resolution in this case is 0.25° (about 20–25 km). Such a resolution is insufficient to accurately consider the effects of mountains on the total dose.
- The SoDa service is primarily oriented toward providing solar (full solar spectrum) radiation dataset mainly for the solar energy domain. For UV it implements the approach developed within the EuroSun project (Wald 2012). This provides UVB and UVA data over the area covered by MSG since its inception (2004) until the current period. Its temporal resolution is excellent (15 min), while the spatial resolution is of the order of 5 km over Switzerland. One disadvantage is that it implements an empirical method that transforms the irradiance integrated over the full solar spectrum (hereafter solar irradiance) into irradiance in the UV bands. The disadvantage is that the sensitivity of solar irradiance to the content of ozone in the atmosphere is limited, while UV irradiance sensitivity to ozone is very high. Thus, such a method cannot reproduce the changes in UV irradiance induced by atmospheric ozone content variability. Furthermore, one of the main factors affecting the daily or yearly irradiance profile is the dependence on solar elevation, which is due to a combination of geometrical effects (the angle between the direct beam and the horizontal surface on which global irradiance is defined) and the amount of atmosphere that is traversed by the direct beam. The geometrical effect is similar for both solar and UV irradiance, but the effect of the amount of atmosphere traversed is markedly different because of the UV absorption by ozone. This results in a different UV dependence on solar elevation and consequently on daily, and more importantly, seasonal cycles that are different for UV and solar irradiance.

- The UV dataset developed for the epidemiology project by (Vienneau et al. 2017) is derived from a climatology of solar irradiance computed with the HelioMont algorithm (Stöckli 2013). The HelioMont algorithm uses several data sources from large-scale datasets, typically from the ECMWF or from the European Organisation for the Exploitation of Meteorological Satellites (EUMETSAT), as inputs to calculate the solar irradiance at the surface. The input data with the highest spatial and temporal variability determines the resolution of the HelioMont output, in this case that is the cloud cover input. For this, HelioMont relies on data from MSG, which can achieve an output spatial resolution as high as about 0.02° (about 2 km in Switzerland). The HelioMont algorithm produces output with a temporal resolution as high as 15 min, but the UV climatology produced by (Vienneau et al. 2017) used long-term monthly averages over the period 2004–2008. In order to derive erythemally weighted UV irradiance estimates from HelioMont solar irradiances, a linear mixed-effects regression model was developed based on UV irradiance at four MeteoSwiss stations and HelioMont estimates at the corresponding locations. Because this empirical model does not account for the effect of ozone, it is affected by the same problems as the SoDa/EuroSun estimates.

Aside from the SoDa/EuroSun product, all the datasets described above have a temporal resolution no finer than one day. This may be sufficient for total dose estimates (bearing in mind the accuracy and precision limitations described above), but it is not sufficient for effective dose estimates.

1.3. Aims of the study

The aim of this study was to develop a new method for producing high quality, satellite-based UV data that meets the requirements for accurate effective dose estimation that can thereafter contribute to a public health, population-based vision of risk. Unlike existing UV data, our climatology is intended to fulfil all the following requirements i) accurately reproduce UV dependencies on the main influencing factors: SZA, cloudiness, atmospheric ozone content, aerosol optical depth (or atmospheric turbidity) and altitude, ii) have a sufficiently high spatial resolution to adequately resolve mountain effects and iii) have a sufficiently high temporal resolution to establish the variation of irradiance during the day that can thereby be used in tandem with ER variation to estimate effective doses.

2. Material and methods

2.1. Satellite data

In order to establish a climatology of ground-level UV radiation fulfilling the requirements laid out above, we applied a method similar to the HelioMont algorithm (Stöckli 2013) or more generally the Heliosat algorithm family (Cano et al., 1986; Möser and Raschke, 1984; Mueller et al., 2004; Posselt et al., 2012, 2014). We chose this approach because it had previously been used to generate a radiation climatology fulfilling our requirements, but for solar radiation *integrated over the full spectrum*. Therefore we adapted the algorithm to use only the UV spectrum range and generate new data instead of using empirical functions to transform the original full spectrum output into UV estimates. The HelioMont or Heliosat algorithm can generate radiation estimates over Europe by using large-scale datasets provided by EUMETSAT, ECMWF, and the Copernicus Atmosphere Monitoring Service (CAMS). These datasets are usually generated by atmospheric models fed with satellite data.

HelioMont calculates surface solar irradiance with a combination of a clear-sky algorithm derived from data generated with the libRadtran RTM (Mayer and Kylling 2005) and a satellite-based cloud-forcing algorithm. The spectral range of libRadtran can be set by the user, e.g. as the full solar spectrum or just the UV spectrum. Adapting this part of the algorithm is thus relatively straightforward. For the cloud forcing, we rely on the findings of UV reconstruction studies. Because historical UV measurement data are extremely scarce, multiple studies use proxy data (typically the atmospheric ozone column, surface albedo and solar radiation) to infer the corresponding historical UV radiation (Bilbao et al., 2011; Bodeker and McKenzie, 1996; den Outer et al., 2005; Kaurola et al., 2010; Koepke et al., 2006; Lindfors and Vuilleumier, 2005). UV reconstruction was the term coined to designate such techniques. While these studies usually show that UV radiation cannot be directly inferred from solar radiation over the full spectrum they show that cloud forcing in the UV range is very well correlated to the cloud forcing for the full solar spectrum. Thus we can combine the libRadtran clear-sky surface UV irradiance and the HelioMont cloud forcing to estimate the *all-sky* surface UV irradiance.

2.2. UV climatology for clear-sky

We derive UV clear-sky irradiances based on the version 2.0 of the libRadtran RTM (Mayer and Kylling 2005) restricted to the UV range (290–400 nm) and with an erythemal action spectrum applied (McKinlay and Diffey 1987). RTM's such as libRadtran have been shown to accurately reproduce functional behaviour of UV irradiance with respect to key parameters (Koepke et al. 2006). However, directly using libRadtran is impractical because of the number of simulations required. We aim at using the best spatial resolution allowed by HelioMont (1/48≈0.02°), resulting in a 103x241 = 24′823 pixel map to cover all Switzerland. We also want to temporally resolve our 15-year climatology at an hourly resolution. In total, this would require about 3 billion libRadtran simulations. Furthermore, the hourly simulation does not adequately resolve the time at sunrise and sunset when irradiance changes very quickly, and a 5-minute resolution is more adequate requiring about 39 billion simulations. An RTM is too computationally intensive for this and methods for reproducing the output of the RTM based on a limited set of the most important simulation input parameters is required. HelioMont, for example, uses a look-up table approach.

In our case, we first used libRadtran for sensitivity studies to select the most important parameters after a first choice based on the available literature. The selected parameters were the SZA (or similarly solar elevation), the total ozone column, the surface albedo, the aerosol optical depth (AOD) as an indicator of atmospheric turbidity, and the altitude as an indication of the amount of atmosphere above the surface. Then, libRadtran was used to generate simulations with each of four of the five parameters given five different values covering the possible range in Europe while AOD was given 20 values. We treated AOD differently because it changes as function of wavelength and as we are interested in UV radiation transfer, we used the AOD at 368 nm as an input parameter. However, the dependence of AOD on wavelength also varies depending on the aerosol type. We did not include a supplementary parameter to account for the type of AOD wavelength dependency because our sensitivity tests showed that this had a limited influence when using as input parameter an AOD at a UV wavelength. Nevertheless, we repeated libRadtran simulations with five AOD value and four different AOD wavelength dependencies to account for small differences resulting from the wavelength dependence. Consequently, we performed $5^4 \times 20 = 12'500$ simulations for all possible combinations of the input parameters.

In order to reproduce the results of libRadtran, we fitted a multidimensional 3rd-order polynomial function on the libRadtran simulation results. The fit variables are the five influential parameters we selected (x_i, $i = 1,\ldots,5$). The polynomial fit function includes all combinations of variables up to the 3rd-order ($1, x_i, x_i x_j, i \le j, x_i x_j x_k, i \le j \le k$). A further refinement was necessary because the UV irradiance does not typically depend on the selected influential parameters in a way easily reproducible with a 3rd-order polynomial. For example, extinction of light through the atmosphere usually results in an exponential decrease in radiation intensity as a function of the length of traversed atmosphere

(at least for the direct beam). Thus, the x_i in the polynomial are in fact functions of the influential parameters, usually involving logarithms.

With the fitted polynomial, libRadtran results can be approximated with simple matrix multiplications which, when optimized efficiently, can lead to millions of simulation results obtained in seconds. The *maximum* differences between the polynomial fit and the libRadtran results over the 12′500 simulations were around 7%. However this was for extreme situations, typically for the sun at the zenith (which never occurs in Switzerland) and a total ozone column of 100 Dobson Units (DU) which is lower than any measurement ever made in Switzerland. For more reasonable values, the differences were below 5%.

Although the input parameters required for this calculation are not trivial, the physical processes simulated by the RTM are well understood and the quality of the estimates is essentially limited by the quality of the input data. In performing the validation later in this paper, we also specifically assess the accuracy of the clear-sky estimation, implicitly considering all uncertainty sources. This includes the representation of the physical processes in libRadtran, the simplified assumptions on input parameters (use of default values for parameters others than the five influential input parameters considered), the approximation of the libRadtran computations with a polynomial fit function and the uncertainties in the five influential input parameters.

2.3. Cloud modification factor

The cloud forcing or equivalently the cloud effect on UV radiation is obtained from HelioMont estimates of this forcing that are corrected for the UV spectrum. For consistency with UV reconstruction terminology, we condense the cloud effect into a Cloud Modification Factor (CMF). Multiplying a clear-sky UV estimate by the CMF corresponding to that time and location yields the all-sky UV estimate. To compute the CMF, HelioMont follows the classical Heliosat approach wherein satellite measured reflectances are contrasted to cloud free (surface) reflectances (Stöckli 2013). For this purpose, HelioMont employs the MSG SEVIRI High Resolution Visible (HRV; 0.45–1.1 μm) channel in combination with five other near-infrared and infrared channels (0.6, 0.8, 1.6, 10.8, 12.0 μm). This provides the 0.02° spatial resolution output characterizing the cloud effect.

Previous authors have shown that the CMF in the UV range can be derived from the CMF for the full solar spectrum (CMF_{SOL}) and the solar zenith angle (den Outer et al. 2010). We use their parameterization 3: $CMF^{HM} = 1 - (1 - CMF_{SOL})^{(1+q)}$, where CMF_{SOL} is the HelioMont-derived solar CMF, CMF^{HM} is the UV CMF, and q is a "curvature" parameter depending on the solar zenith angle. Once the clear-sky UV estimate (UV_{cs}) and the CMF^{HM} are available, the all-sky estimate is $UV_{as} = UV_{cs} \cdot CMF^{HM}$. Due to the particular HelioMont information used in this study, the CMF^{HM} is defined at an hourly temporal resolution. The UV_{cs}, which is defined at 5 min resolution, must therefore be averaged across each hour to compute UV_{as} with hourly resolution.

2.4. Model validation

We validated our UV climatology by comparing its surface UV irradiance estimates with ground-based irradiance measurements. For the validation, we needed measurements of UV global irradiance with erythemal weighting as well as measurements of the broadband full solar spectrum global irradiance and diffuse irradiance. The UV global irradiance is the validation data and the full solar spectrum global and diffuse irradiance are used to determine clear-sky times with a dedicated algorithm (Long and Ackerman 2000).

Such data are measured at three stations in Switzerland: Davos, Locarno-Monti and Payerne. At each station, compliance with the guidelines of the Baseline Surface Radiation Network (BSRN) (Ohmura et al. 1998) ensures high data quality. Payerne (PAY, 46.81°N, 6.94°E, 491 m ASL) is the Swiss BSRN station and is located on the Swiss plateau. Davos (DAV, 46.81°N, 9.84°E, 1610 m ASL) is located in an alpine valley, and Locarno (LOC, 46.18°N, 8.78°E, 366 m ASL) is located in the lowlands south of the Alps. At all stations the measurement program started before the beginning of our UV climatology (2004). The data are measured every minute, although DAV and LOC were measured every two minutes at the beginning of the measurement program. Because of upgrades of measurement station infrastructure, or in one case the maintenance of a building, there are measurement data gaps, but at each station, there are more than 10 years of common UV climatology estimates and ground-measured data.

UV measurements are performed using broadband UV radiometers (Biometer 501A, Solar Light Company Inc., Glenside, PA, U.S.A.) with filters mimicking the erythemal response. These broadband radiometers undergo strict quality assurance procedures, including yearly calibrations traceable to the European Ultraviolet Calibration Centre (Hulsen and Grobner 2007), and the overall uncertainty of the measurement is estimated at 10%.

We first validate our climatology by directly comparing the hourly climatology estimates for the pixel at the location of the three stations to the corresponding hourly averages of the UV measurements. This allows determining agreement statistics such as RMSE or the slope and zero-intercept of a linear regression between measurements and climatology estimates. Because of the determination of clear-sky times by the dedicated algorithm (Long and Ackerman 2000), we can determine such statistics for clear-sky cases alone or for all-sky cases (including both clear-sky and cloudy situations). The clear-sky algorithm identifies clear-sky times for every minute (or two minutes for measurements taken with this time step). Hourly averages are classified as clear-sky if 90% or more of the hour has been identified as clear-sky.

Beyond the direct comparison, the use of a validation CMF provides more insight for evaluating the quality of the UV climatology (Vuilleumier et al. 2020). We define the validation CMF as:

$CMF^{val} = UV^{meas}/UV_{cs}$, where UV^{meas} are the measurements at the three stations and UV_{cs} are the clear-sky estimates described in the beginning of the section for the pixels corresponding to the stations. Since clear-sky estimates are computed every 5 min, they can be interpolated for every minute resulting in corresponding CMF^{val} for every ground-based measurements. We then compute hourly averages of CMF^{val} for the validation. The validation CMF provides insight for both clear-sky cases and the treatment of the cloud effect.

For clear-sky cases, it is actually more appropriate to use the inverse of CMF^{val}, which compares our theoretical estimate UV_{cs} to the corresponding clear-sky measurement UV_{cs}^{meas}. Ideally, the inverse of CMF_{cs}^{val} should be equal to 1, and the width of the distribution around 1 is an indication of its uncertainty, while the difference between the distribution average and 1 allows estimating the average bias. A previous study (Vuilleumier et al. 2020) showed that the width of the distribution of $1/CMF_{cs}^{val}$ is the result of the combination of the relative UV_{cs} uncertainty and the relative UV_{cs}^{meas} uncertainty, under the assumption that the uncertainty contributions to the variance can be linearized and that they are statistically well behaved. Since we know the uncertainty of UV_{cs}^{meas}, we can deduce the uncertainty of UV_{cs}. This analysis avoid a caveat of the direct comparison between climatology and measured values. Because the main factor determining the clear-sky UV is the solar elevation or solar zenith angle (UV radiation is higher in summer than winter and higher at midday than at beginning or end of day), the correlation between modelled and measured clear-sky UV is often misleadingly high and somewhat meaningless. Since the computation of UV_{cs} includes the solar zenith angle that can be determined with a high accuracy, $1/CMF_{cs}^{val}$ is a normalized quantity whose deviation from 1 shows the uncertainty due to factor beyond the solar zenith angle.

In all-sky cases, the CMF can take value from a minimum slightly above zero (of the order of 0.01, which means clouds are almost completely suppressing radiation) to maximal values a little above unity (up to 1.2–1.3 in case clouds are not blocking direct radiation while

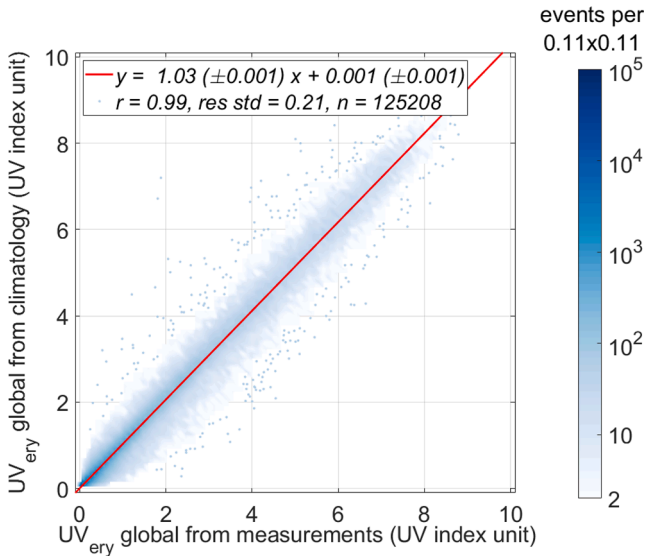

Fig. 1. Comparison between satellite-derived UV estimates and measured UV at Payerne, all-sky conditions, period 01.2014–10.2018 (n = 125′208). The figure is divided in squares of 0.11x0.11 UVI and a logarithmic colour scale indicates the density of points per square. When less than two points per square are present the individual points are shown.

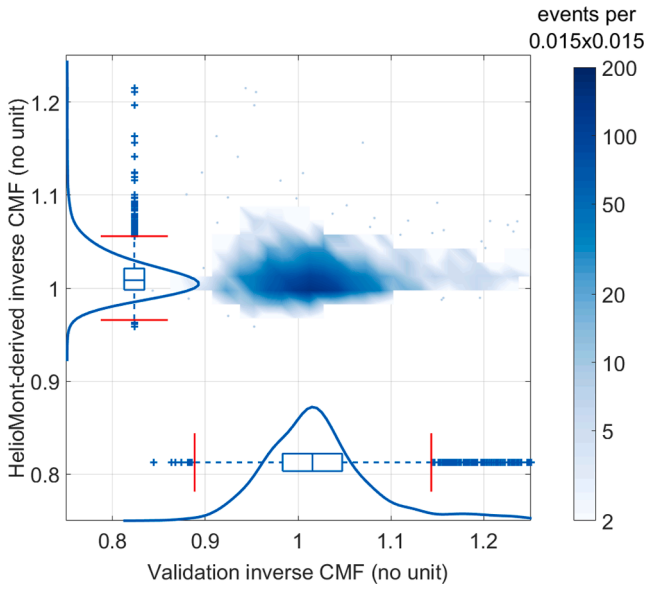

Fig. 2. Distributions of inverse cloud modification factor (CMF) for clear-sky cases at Davos, period 01.2004–10.2018 (n = 2′469 hourly averages). The 2-dimensional distribution (CMF_{cs}^{HM} vs. CMF_{cs}^{val}) is shown in the same way as in Fig. 1, and the 1-dimensional distributions are represented with boxplots and PDF along the x-axis (CMF_{cs}^{val}) and y-axis (CMF_{cs}^{HM}). The boxplots show the median, interquartile range and whiskers that extend to the 25th percentile minus 1.5 the interquartile range and the 75th percentile plus 1.5 the interquartile range. The PDF are derived using a kernel normal density estimator.

enhancing diffuse radiation). Comparing the all-sky CMF_{as}^{HM} to CMF_{as}^{val} allows validating the accuracy of the cloud treatment by the HelioMont algorithm and the subsequent conversion to the UV range. However, in this validation step the uncertainty of the validation value CMF_{as}^{val}, determined from the previous step, must also be considered.

3. Results

The climatology extends from 01.01.2004 to 31.10.2018 at a temporal resolution of 1 h and a spatial resolution of 0.02° (about 1.5 to 2 km, depending on the direction). There is no large data gap and the amount of missing data is <2% (missing UV climatology data result from missing input data for the algorithm described in section 2).

3.1. Validation of the climatology dataset

The good correspondence between the UV climatology estimates and the ground-based measurements is shown in Fig. 1 for Payerne as an example. A logarithmic density plot shows the comparison between UV climatology estimates and measurements at the MeteoSwiss station Payerne (46.8°N, 6.9°E, altitude 491 m) for all hourly averages of the climatology when measurements were available (all-sky conditions, n = 125′208). The linear regression fit has a slope of 1.03 compatible with estimates agreeing with measurements on *average* (measurement uncertainty is about 10%). The standard deviation of the residuals to the regression line is about 0.2 UVI units and the RMSE is 0.214 (strictly speaking this is a root mean square difference – RMSD, because UV_{as}^{meas} is not the true value, but is affected by measurement uncertainty). The dispersion around the regression line does not decrease when the UV values decrease, except for almost zero values. Low all-sky UV values are either due to conditions that would produce low clear-sky values (winter or beginning and end of day) or to low CMF (high cloudiness).

The distribution of the differences between the climatology and the measurements can first be analysed for a better understanding of the climatology uncertainty, but these distributions show the combined effect of the climatology and measurement uncertainty. Thus the difference distributions are very conservative estimates of the UV climatology uncertainty. When considering all daytime data (SZA < 86°) together, about 90% of the hourly differences are within ± 0.5 UVI, which can be considered as an expanded uncertainty value for the UV climatology. However, most of the values are small (the median UVI is typically around 1), because this includes all cases when the sun elevation is low or there are clouds. When distributing the data in classes of low (0–3), median (3–6) or high UVI (>6), about 90 percent of the differences are included within ± 0.3 for low UVI, within ± 1 for median UVI, and within ± 1.5 for high UVI. As a relative uncertainty, this represents about ± 50–60% for low UVI, ±25-30% for median UVI, and ± 15–20% for high UVI. This increased relative uncertainty for low UVI characterizes all-sky values. When clear-sky times are selected, the corresponding relative uncertainties only decrease from about ± 15–20% for low UVI to ± 10–15% for high UVI.

The results of the comparisons between UV climatology estimates and the ground-based measurements are quite consistent between stations. Table 1 gives the statistical indicators for the UV all-sky comparisons described above in Fig. 1 for the three MeteoSwiss stations. At

Table 1
Agreement statistical indicators for the comparisons between all-sky UV estimates and measurements.

Station [a]	Regression slope [b]	Regression zero intercept [c]	Residual standard deviation [c]	RMSD [c]	Pearson correlation coefficient [b]	Number of events
Locarno	1.04	0.001	0.216	0.231	0.991	115′998
Payerne	1.03	0.001	0.208	0.214	0.991	125′208
Davos	0.95	0.017	0.307	0.323	0.982	90′899

[a] in order of increasing altitude
[b] no unit
[c] UVI unit

Table 2
Width of the distribution of clear-sky inverse validation CMF, period 01.2014–10.2018; range min and max indicate the boxplot whiskers and % in range indicates the percentage of events within this range.

Station [a]	range min	25% tile	average	median	75% tile	range max	% in range
Locarno	0.91	1.03	1.08	1.08	1.12	1.25	88.4
Payerne	0.90	1.00	1.04	1.04	1.07	1.17	92.3
Davos	0.89	0.98	1.02	1.01	1.05	1.14	92.5

[a] in order of increasing altitude

Locarno the results are similar to Payerne. Differences compared to Davos might be due to a higher uncertainty coming from the surface albedo (more frequent snowy conditions) and Davos' topography being in an alpine valley.

As mentioned in section 2, analysing the distribution of the inverse CMF for clear-sky events allows determining the accuracy of the clear-sky part of the algorithm generating the climatology. Fig. 2 shows the distributions of $1/\mathrm{CMF}_{cs}^{val}$ along the *x*-axis and $1/\mathrm{CMF}_{cs}^{HM}$ along the *y*-axis for Davos. Ideally, all the CMF values should be 1. For CMF_{cs}^{HM}, the distribution is narrow and well centered around 1. This means that HelioMont finds a CMF around 1 (corresponding to clear-sky) for events that are selected as clear-sky by the algorithm of (Long and Ackerman 2000). The opposite is not true as data attributed a CMF around 1 by HelioMont are not all selected by the clear-sky algorithm. The width of the distribution of $1/\mathrm{CMF}_{cs}^{val}$ is due to the combination of the relative UV_{cs} uncertainty and the relative UV_{cs}^{meas} uncertainty (Vuilleumier et al. 2020), and the range between the whiskers of the corresponding boxplot on Fig. 2 is a robust non-parametric estimate of the expanded uncertainty.

Table 2 indicates quantiles and the range covered by the boxplot whiskers for the distributions of $1/\mathrm{CMF}_{cs}^{val}$ at the three stations. The median is between 1.01 and 1.08 and the distribution is in large part included in a range of ± 12% to ± 17% from the median (the last column of Table 2 indicates what percentage of clear-sky cases are within the range defined by the whiskers). This confirms the results of the analysis of the difference distributions for clear-sky cases. Considering that the expanded relative UV_{cs}^{meas} uncertainty is about 10%, the expanded relative uncertainty on UV_{cs} should be of the order of 10% to 15%.

Fig. 3 compares, for all-sky situations, the HelioMont-derived CMF_{as}^{HM} to the validation CMF_{as}^{val} for Payerne, excluding all situations with solar

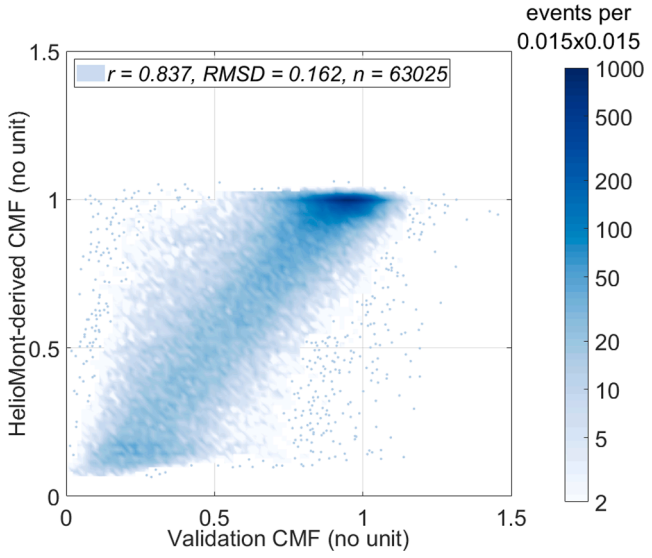

Fig. 3. Comparison between HelioMont-derived CMF and validation CMF obtained at Payerne, 1 h average, solar zenith angle < 85°, period 01.2014–10.2018 (n = 63′025).

Table 3
Agreement statistical indicators for the comparisons between all-sky HelioMont-derived CMF and validation CMF.

Station [a]	RMSD [c]	Pearson correlation coefficient [b]	Number of events
Locarno	0.177	0.849	57′835
Payerne	0.162	0.837	63′025
Davos	0.163	0.774	45′673

[a] in order of increasing altitude
[b] no unit
[c] UVI unit

zenith angle higher than 85°. (It is not meaningful to compute validation CMF during night; in addition, at low solar elevation, it is extremely difficult to infer the cloud effect from satellite imagery because of the large difference between viewing and solar angle). Considering the difficulty of inferring the effect of cloud on radiation from satellite imagery and the supplementary uncertainty introduced by the transformation from the visible to the UV range, the agreement is relatively good. The correlation is about 0.77–0.85 (based on Pearson correlation coefficient *r*, Table 3 gives *r* and RMSD for all stations), while the RMSD is between 0.16 and 0.18 for a quantity typically between 0 and 1. Since RMSD is a quantity that would relate to standard and not expanded uncertainty, the treatment of the cloud effect in the algorithm generating the climatology is the main component of the uncertainty for the estimation of the all-sky UV irradiance.

A region of high density is visible for $\mathrm{CMF}_{as}^{HM} \sim 1$ and $0.7 < \mathrm{CMF}_{as}^{val} < 1.1$ on Fig. 3 . It is partly due to the uncertainty in the clear-sky determination, but this would only justify this region extending down to ~ 0.85. The fact that this region extends down to ~ 0.7 may be due to thin clouds that are not detected by HelioMont, but influence the measured radiation. In general, for high CMF, the algorithm seems to overestimate the CMF (data are mostly above the diagonal). Because a CMF of 1 means the cloud has no effect and a CMF of 0 means a cloud totally blocks radiation, it means that the cloud effect is underestimated in good-weather situation. On the other hand, at low CMF (high cloud coverage), the algorithm seems to underestimate the CMF (data mostly below the diagonal) and the cloud effect is consequently overestimated for high cloudiness. The reason for this behaviour is unknown, but it is seen at the three stations.

3.2. Comparison to other UV climatology datasets

Beyond validating our climatology with respect to surface data, comparisons can also be made to other available datasets. From those mentioned in the introduction, the ones produced by the SoDa service and the COST Action 726 are of particular interest because they are available online and fully cover the same geographic area. There are some limitations nonetheless: the COST Action 726 dataset is only available at a daily time resolution and it is computed up to August 2002, so it does not temporally overlap with our climatology. The SoDa dataset is available at temporal resolution as fine as 15 min, however its web site warns that the method used (Wald 2012) is only demonstrated at a daily resolution and findings deduced from its intraday variability should be used with caution. We should thus only compare results derived at a daily resolution.

For the COST Action 726 dataset, the most pertinent comparison is the one between mean annual cycles derived from all UV climatology datasets. We compared these with the equivalent annual cycle derived from surface measurements at the three validation meteorological stations. UV time series of comparable length were extracted from the surface measurements datasets of Locarno, Payerne and Davos. The extracted periods were, for our climatology, January 2004 to October 2018, for the SoDa climatology, February 2004 to December 2018, for the COST Action 726 climatology, January 1990 to August 2002 and for surface measurements, January 2004 to October 2018. The time series from our dataset, the SoDa dataset and the ground measurements are

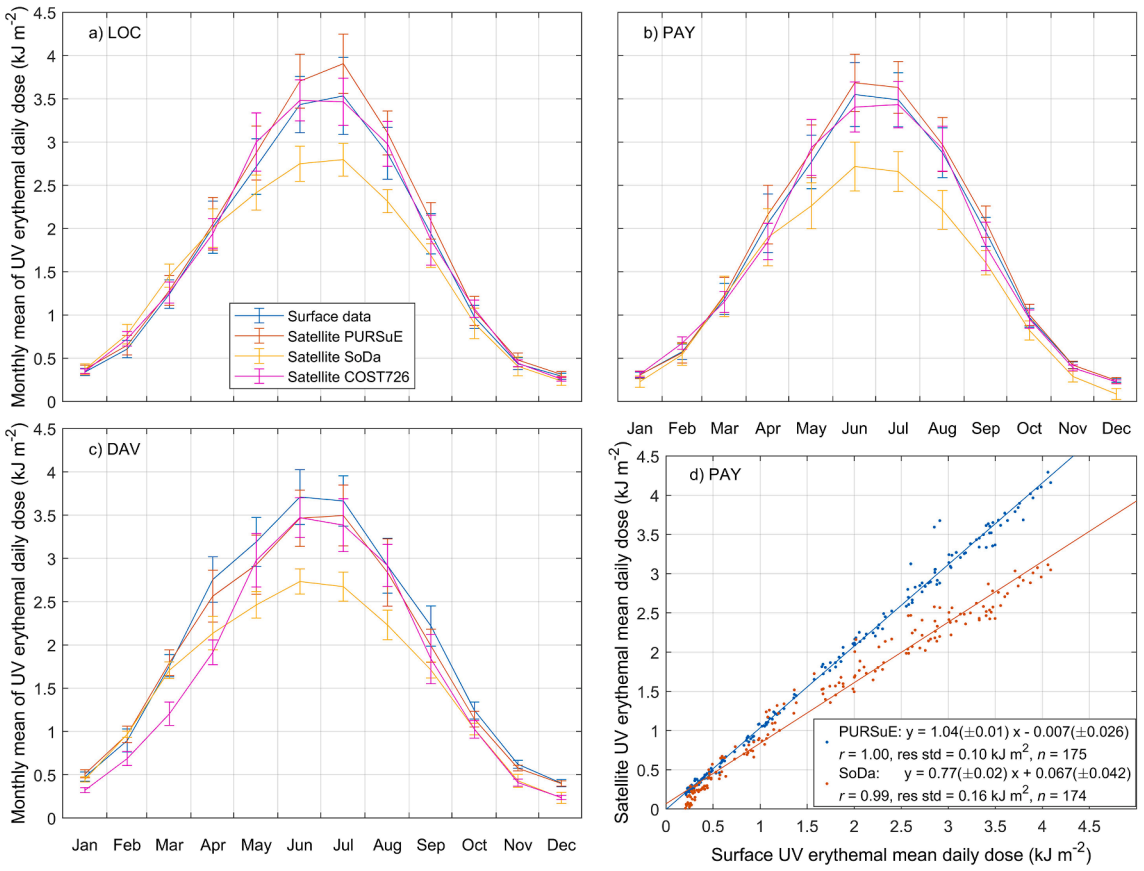

Fig. 4. Comparison between mean annual cycles from our satellite climatology (PuRSUE), from the SoDa climatology, from the COST Action 726 climatology and derived from surface data for a) Locarno, (LOC), b) Payerne (PAY) and c) Davos. (DAV). The error bars show, for each month of the year, the standard deviation through all years in the datasets for the given month. d) Month by month comparisons with surface measurements for our climatology and the Soda climatology at Payerne.

approximately for the same period and so month by month comparisons can be made. However, the SoDa dataset only provides data for UV radiation spectrally integrated over the UVA and UVB range, and not for UV with an erythemal weighting. To allow comparisons, we derived corresponding UV erythemally-weighted data from the SoDa UVA and UVB data using a multiple regression analysis.

For the COST Action 726, the annual cycles should be compared under the assumption that the overall climatology of UV radiation did not evolve significantly from the end of the period covered by COST Action 726. (Bilbao et al., 2011; Bodeker and McKenzie, 1996; den Outer et al., 2005; Kaurola et al., 2010; Koepke et al., 2006; Lindfors and Vuilleumier, 2005) showed that between 1980 and 2000 UV radiation should have increased in Switzerland by about 4% to 5% per decade in average, mainly because of the decrease in the total ozone column. Since the period covered by the time series from COST Action 726 precedes the period covered by the other time series by a little more than 10 years, there may be a difference of roughly 5% (COST Action 726 lower than the others) attributable to the evolution of UV radiation if the trend observed from 1980 to 2000 continued through to 2018.

For the comparisons, we first computed the total UV erythemal daily dose on a horizontal surface in kJ m^{-2} for each time series. We then computed the monthly mean of the daily doses for all months in the datasets. Finally, for each time series we computed mean annual cycles by averaging all months of January together, all months of February together, etc.

Fig. 4 shows the annual cycles of the monthly means of the UV daily doses for all datasets at Locarno, Payerne and Davos (a–c). Fig. 4d shows a satellite vs. surface month by month comparison for our climatology and the SoDa climatology at Payerne. For our climatology, the largest relative differences from the surface measurements are in summer at Locarno (10.5% for July, (satellite – surface) / surface). At this station our climatology seems systematically overestimated by 1.9% to 10.5% depending on the month. At the other stations, the differences are more equally distributed (Payerne between −2.0% and 6.1%, Davos between −10.3% and 7.7%). Such differences are within measurement uncertainty. However, the averaging process should strongly reduce the statistical component of the uncertainty, and so some of these differences may be significant. (This is likely the case at Locarno since the overestimation is systematic over the annual cycle). At the other stations, there is no systematic difference and our satellite estimates seem to provide average values within 10% from measurements, while at Locarno one month differed by 10.5%. This is confirmed by month-by-month comparisons (see Fig. 4d for Payerne).

The annual cycles derived from the SoDa climatology show systematic underestimation by −20% to –25% in summer at all stations. Since the highest UV radiation levels are experienced in summer, these are also the largest absolute differences. The relative differences for SoDa are −20.9% to + 28.3% at Locarno, −64.5% (in December) to + 2.5% at Payerne and −42.2% (in December) to + 8.0% at Davos. Such discrepancies are likely due to SoDa using an empirical method transforming the irradiance integrated over the full solar spectrum into irradiance in the UV bands, which does not correctly represent the dependency to ozone as mentioned in the introduction.

The annual cycles derived from the COST Action 726 climatology are remarkably close to those derived from the surface measurements considering the coarse spatial resolution (1°) and the different periods analysed. The relative differences are −11.5% to + 19.5% at Locarno, −10.2% to + 17.6% at Payerne and −41.0% (in December) to + 0.2% at Davos. Given these differences, the possible systematic effect of about 5% due to the evolution of UV radiation is negligible. The most visible difference is at Davos from January to April, where COST Action 726

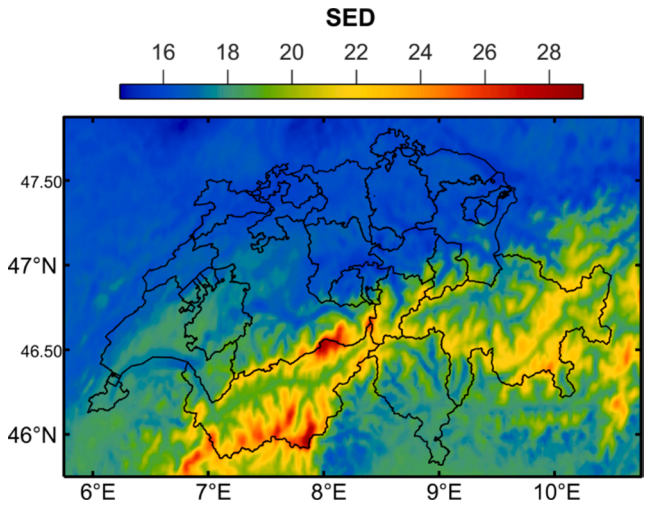

Fig. 5. Map of average all-sky UV erythemal daily doses (SED) across Switzerland. UV daily doses (24 h exposure) are computed for every pixel and every day of the 15-year climatology and a temporal average over all days is computed for each pixel. The map of Switzerland is given on a longitude, latitude grid.

systematically underestimates the UV radiation. It should be noted that the Davos cycle from surface data is significantly asymmetric with respect to the maximum in June-July with more radiation in spring than in autumn, a feature that COST Action 726 fails to represent. This is due to snow accumulating in winter and slowly melting in spring at this mountain station. The persistent snow affects the surface albedo and consequently the UV radiation. For surface albedo, our method uses an empirical derivation based on the HelioMont estimation of the surface reflectance in the visible. HelioMont uses a refined determination based not only on the visible channels of MSG but also on its near-infrared and infrared channels to improve the discrimination of cloud and surface reflectance for bright surfaces (snow). This allows our UV climatology to accurately reproduce this feature of the annual cycle at Davos where COST Action 726 cannot.

3.3. Visualizing climatology data

Sections 3.1 and 3.2 aimed at establishing how accurate the UV climatology is. Below, we give examples of its use. These examples give a succinct overview of the versatility of the type of information that can be derived from the climatology. These examples illustrate possible uses of a spatially and temporally extended UVR dataset in an environmental perspective, considering both chronic (average daily doses) and acute exposure (extreme values) indicators. As the metric used here is derived from the UV_{ery} irradiance at ground level, one should keep in mind that it refers to a maximal exposure and thus surrogating a potential risk.

Fig. 5 shows for every pixel the average UV daily dose on a flat horizontal surface expressed in standard erythemal dose (SED). First the UV daily dose is computed by integrating the average UV irradiance of the 24 h for each pixel and each day of the 15-year climatology and then a temporal average over all days is computed for each pixel. The time resolution of the climatology also allows computing more specific exposures, for instance selecting only days of specific months to compute average exposure in June for example, or at a specific time of day, for example for computing average dose for an exposure in June between 10:00 and 14:00 (the climatology uses UTC times, but the data extraction tool we created has an option for local time, including daylight saving time, if desired). The average daily doses in Fig. 5 are between 15 and 29 SED and the spatial variability is mainly related to topography with highest doses at mountain tops and ridges, while lowest doses are found in lowlands and valleys. The Alps are approximately in the South-East half of Switzerland, and it is where the highest doses are found. There are three reasons that explain why UV intensity is higher in mountains: the atmosphere traversed by UV radiation is thinner, there is less cloudiness above high mountains (when low clouds are present

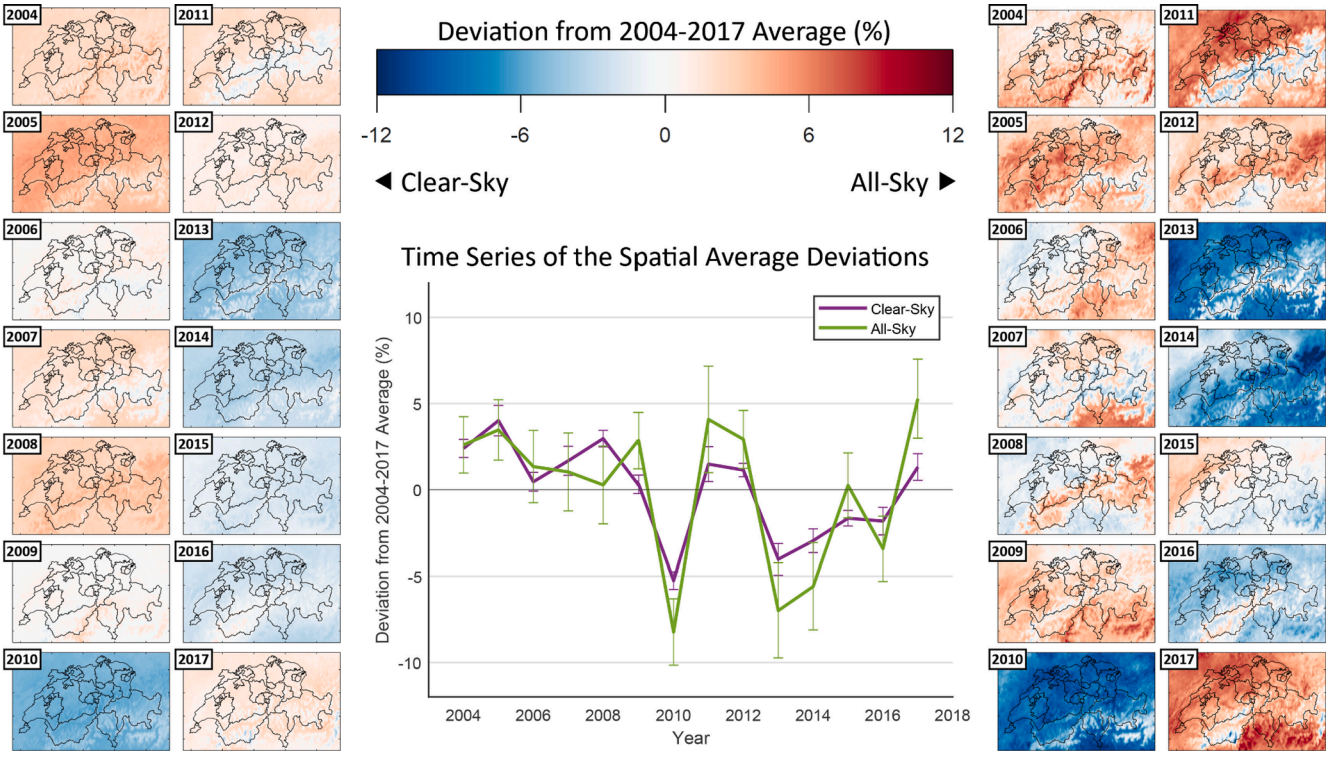

Fig. 6. Yearly deviations of average all-sky UV erythemal daily doses (SED) across Switzerland. UV daily doses for each pixels are computed similarly to Fig. 5, but annual averages of the doses are first computed and the deviation to the 2004–2017 averages is then computed for each pixel. Annual deviations for clear-sky are given on the left and for all-sky on the right. On the middle panel the evolution of spatial average of yearly deviations is shown.

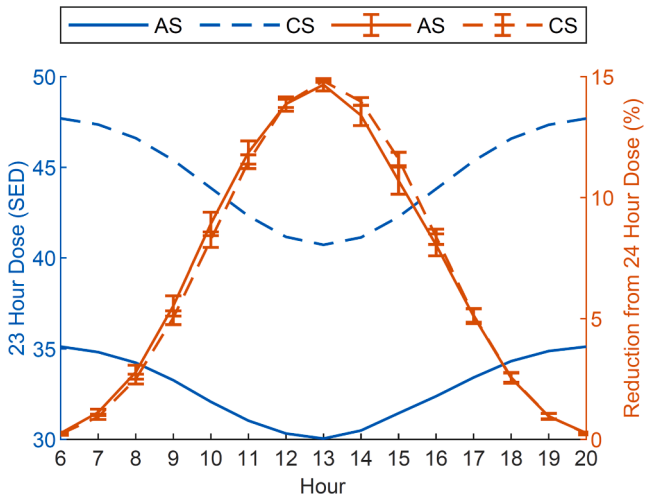

Fig. 7. Average dose reduction incurred by staying one hour unexposed (e.g., staying indoor) with respect to average daily dose in June. The total daily dose with one hour unexposed is indicated in blue (solid line for all-sky and dashed line for clear-sky, left-axis scale) as a function of the hour when the exposure is avoided. The relative reduction is indicated in red (solid line for all-sky and dashed line for clear-sky, right-axis scale). (For interpretation of the references to colour in this figure legend, the reader is referred to the web version of this article.)

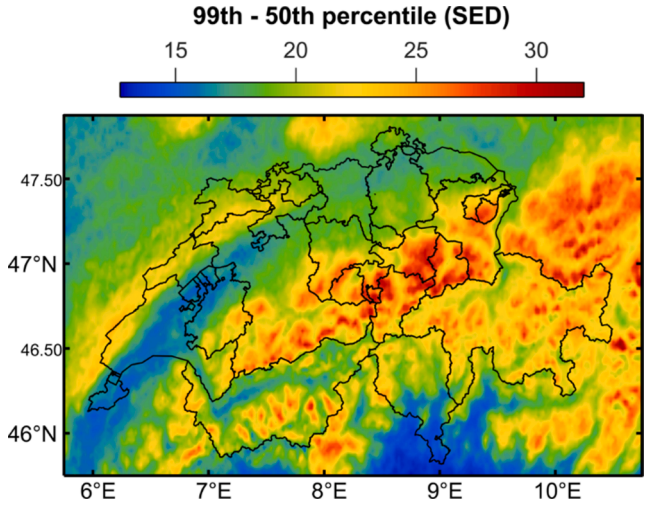

Fig. 8. Map of differences between 99th percentile and median of all-sky UV erythemal daily doses (SED) across Switzerland for June. UV daily doses (24 h exposure) are computed for every pixel and every June day of the 15-year climatology and the difference between the 99th percentile and the median is computed for each pixel. The map of Switzerland is given on a longitude, latitude grid.

mountain tops and ridges are above the cloud layer) and the surface albedo is higher due to snow. Since we first compute clear-sky UV irradiances and then apply a cloud method factor accounting for the effects of clouds, we also have a clear-sky UV climatology that gives an idea of what are typical maximum values when clouds are not present. A similar figure, but for clear-sky average doses, is given in the Appendix.

Fig. 6 represents the year-to-year variability of the annual averages of the UV daily doses with respect to the averages over the period 2004–2017. (Since the climatology includes only 10 months of 2018, this figure is restricted to the period 2004–2017; it makes only a negligible difference for the overall average, but it makes a significant difference on the 2018 averages because two winter months are excluded). The year-to-year differences are shown as maps on the left for clear-sky (Fig. A.1. shows the average doses over the full climatology period) and on the right for all-sky (i.e., considering the effect of cloud, corresponding to Fig. 5). The evolution of the spatial average of the yearly differences (over all pixels) is shown on the middle panel for both clear-sky and all-sky results, and the standard deviations over all pixels are shown as error bars (±1 standard deviation). The main source of variability for clear-sky data is ozone, while for all-sky data, year-to-year variation in cloud cover also plays a significant role. Fig. 6 shows that year-to-year variability for individual pixels is within about ± 10%, while it is restricted to about ± 5% when averaged over all Switzerland. As expected, the variability is stronger when the effect of cloud is taken into account (all-sky data), especially at the pixel level.

For risk prevention it may be important to assess the dose reduction incurred by avoiding exposure during a certain time. In Fig. 7, we show the effect of avoiding exposure during one hour at different time of day for the month of June. In this case we computed the average daily dose over all June days in the climatology and all pixels, but we repeated the computation 16 times, excluding each time another hour of the day (there are 16 h with daylight in June). We used both clear-sky (dashed lines) and all-sky data (solid lines). The most striking feature is how similar the relative reductions are for clear-sky and all-sky. This means that the effect of cloud is in average homogenous and random. It was expected that an imbalance may occur between morning and afternoon for all-sky data because some clouds (convective clouds) have a tendency to develop in the second part of the day. The all-sky relative reduction is indeed slightly lower during the afternoon than the clear-sky reduction, but the difference is at maximum a couple percent. Confirming that this difference is indeed due to convective clouds would require identification of the cloud type by remote sensing, which is not available in the climatology. For relative risk reduction, error bars show ± 1 standard deviation over all pixels. The error bars are also at maximum a couple percent showing that when averaging over all June days in the climatology, the effect of clouds is also spatially homogenous *when considering relative dose reduction*. Thus for this type of application, clear-sky modelling may be considered instead of using a realistic climatology.

The previous examples are pertinent if one explores issues related to chronic exposure because we computed average doses. In case one is interested in acute exposure, it is more pertinent to study extrema. We computed the difference between the 99th percentile and the median for daily doses for June that are shown on Fig. 8. This indicates, for the month of June, where there is the most difference between a "usual" day and an exceptionally sunny day. First UV daily doses were computed for each pixel and each day that was part of a month of June for the 15-year climatology and then the difference between the 99th percentile and the median was computed for each pixel. Extrema such as 99th percentile are essentially UV doses for clear-sky days. Thus the spatial variability is mainly linked to the effect of clouds on the median, and the largest differences will be found where there is usually more cloud cover. There are two large valleys in the Swiss Alps: the Rhone and the Rhine valleys. The Rhone begins approximately in the middle of the Swiss Alps, flows southwest and then after a bend at lon. ≈ 7°E, lat. ≈ 46.1°N flows northwest; it is clearly visible in bluer colour. The Rhine starts close to the Rhone and flows northeast and after a bend near the eastern Swiss border flows northwest. There are two large chains of mountain tops and ridges on the north and south side of these valleys. These ridges are high enough to often block clouds, and because of weather patterns the north side of these is a location with high cloudiness. The highest differences are found in this region since it is already a mountainous region and clear-sky UV doses are high, but the strong cloudiness lowers the median.

4. Discussion

This paper introduces a novel, freely available, validated and accurate erythemally-weighted UV climatology covering hourly values over 15 years. The resolution of 1.5 to 2 km across Switzerland permits unique estimations of doses received in various geographical locations.

Table 4
Examples of the application of climatology in a health context.

Context	Purpose	Risk situation	Possible indicator
Primary and secondary prevention	Targeting at-risk populations or regions	Health outcomes linked to chronic exposure (e.g. SCC, skin ageing)	Yearly average, multiple year average
		Health outcomes linked to intermittent or acute exposures (e.g. CMM, BCC)	Daily dose, hourly dose, Frequency of extreme events per year
	Targeting at-risk activities (e.g. skiing, seasonal outdoor work) or periods	Chronic exposure	Monthly average, seasonal average, monthly average evolution
		Intermittent or acute exposures	Daily dose, hourly dose, Frequency of extreme events per activity period
Research	Analysing long term exposure pattern, dose response in exposed populations	Chronic exposure	Multiple year average, yearly evolution
		Intermittent or acute exposures	Frequency of extreme events per year

It addresses spatial and temporal shortcomings existing in currently available similar datasets. A careful validation was conducted using independent ground UV data measured at three stations covering the entire temporal extent of the climatology. As the measurements stations represent different environments in Switzerland (an Alpine valley and lowlands north and south of the Alps), the validation accuracy assessment can be extended to the whole climatology. The presented climatology closes an important knowledge gap in estimating the prevalence of solar UV exposure in different populations and estimating the burden of disease of solar UVR since existing dosimetry research has used a variety of methodologies making it difficult to compare studies. Additionally, our analysis shows the importance of considering the effects of clouds when estimating UV. Improving the estimation of the cloud effect is the most promising way of improving the quality of the UV climatology as well as a better understanding of UV exposure and related health outcomes.

As demonstrated by the validation, the climatology is a credible proxy for ground-based UV measurement. Its spatial and temporal resolution also makes it an interesting alternative to dosimetry measurements and provides useful UV maps and data tables for public health purposes. On the one hand, dosimetry has the advantage of measuring an effective dose, and is therefore closer to an individual's biological UV dose (and thus their effective risk). On the other hand, dosimetry has several limits: (1) results are influenced by the way the dosimeters are worn; (2) its broad implementation (at population level or over long period) is extremely resource-consuming, and (3) it exhibits a large variability, which is difficult to interpret for effective public health use. This variability is mainly due to different climate conditions during measurement days, various body sites chosen, short measurement periods and spatial movements during the measurement. Our dataset addresses these various shortcomings of the dosimetry approach by enabling the estimation of short-term and long-term exposure in a methodologically consistent way but, unlike other UV datasets, these advantages do not come with any significant sacrifices to the potential accuracy of dose estimations (i.e. by ignoring cloud effects or using coarse spatial or temporal resolution). Moreover, the use of climatology or satellite data allows one to estimate exposure within minutes compared to dosimetry measurements which may need weeks- or months-long campaigns (Modenese et al. 2019).

The examples given in the results sections demonstrate that the climatology is highly versatile in the way the data can be used and represented, thus it can be tailored to specific research or health outcome goals. A synthetic example of the different indicators and metrics that can be used for public health research and prevention is shown in Table 4. Our climatology can be used to calculate any of the indicators listed and, in most cases, maps can be produced to represent the geographical distribution of risk. The ability to map this information is a key advantage of a climatology-driven approach to public health research and prevention campaigns as it allows experts to more easily identify populations and areas where the potential health risks associated with UV exposure are highest. It can also be used to predict the impact (in terms of exposure reduction) of the possible introduction of certain preventive measures (e.g. the provision of shade for outdoor workers). The versatility of our climatology as an alternative to dosimetry campaigns and as a basis for calculating a variety of risk-related indicators and maps is unmatched in this line of research.

Using our climatology, epidemiologists can cross-reference data from tumour registries with exposure doses considering various temporalities (long term dose, subacute and acute). BCC and SCC have been linked to chronic exposure while CMM has been linked to acute exposures (e.g. sunburns). The relationship between the exposure pattern and the skin cancer occurrence remains poorly elucidated due to the lack of temporally-well-resolved data. Currently available UV datasets cover some but not all of these aspects. Additionally, the extended period covered by our climatology provides numerous novel analysis approaches to better understand public health threats potentially linked to solar UV exposure (as viral infections (HPV), cancer (skin cancer, leukaemia), ocular diseases (cataracts), skin aging or immunosuppression).

The data set for now still faces some limitations for public health use. To estimate effective exposure received, it needs to be combined to exposure ratio modelling based on in-field observations or simulations, hence refining the exposure proxy to get closer to the actual exposure (and thus the actual risk). Further tailoring of the data for public health purposes is planned, including: integrating specific exposure schedules accounting for scenarios with times spent indoor vs. outdoor; exposure ratios (Vernez et al. 2015) accounting for different orientations of body parts with respect to the sun or with different protective measures (Backes et al. 2018), and mapping with spatial information relevant to risk assessment (e.g. population density).

The methodology described can be applied in other countries to develop comparable UV datasets. Data of this quality opens up a wealth of epidemiological and public health research possibilities. With this we hope to contribute to a next generation support system to effectively protect health and advise on achieving a balanced level of UV exposure. Considering that satellite data are available with almost complete global coverage, the same methodology can be used to build up climatology for numerous other countries. The estimation of clear-sky UV radiation requires input data for the total ozone column and aerosol optical depth, which were obtained from databases with global coverage. It also requires elevation maps that are also available globally and the solar zenith angle that can be computed from location and time. Finally, the surface albedo is also required and information on this parameter at UV wavelengths is extremely scarce. In our case, based on measurements at Payerne and literature information, we used an empirical derivation of the UV surface albedo from the albedo for visible wavelengths. Since the visible albedo is an information used by algorithm such as HelioMont, we used the HelioMont visible albedo empirically transformed to UV wavelengths. In the absence of snow, the UV albedo is very low for most surfaces, and a fixed value of about 0.03 could be used to reproduce most of our ground measurements at Payerne and Locarno. At Davos in the Alps, using a fixed value did not allow reproducing our measurements, showing the

importance of the snow coverage. Extending the methodology to other countries experiencing snow coverage will require solutions similar to ours for inferring the surface UV albedo.

After estimating clear-sky values, the CMF must be obtained. Meteorological satellites provide the most adequate information. Because HelioMont is designed to use MSG information, our methodology can be applied to the whole MSG disk that include most Europe and a large part of Africa[1]. Using meteorological satellites other than MSG for other regions will require adapting the algorithm to the satellite data characteristics.

4.1. Conclusions and perspectives

This newly developed and validated UV climatology based on satellite data and having a high accuracy promises to be highly beneficial for international public health. It offers opportunities for new national prevention intervention by enabling researchers and policy-makers to better focus on populations at risk and tailor their approach to meet specific objectives. Furthermore, it represents a unique data source for future studies aiming at linking UV exposures to long term evolution, such as climate change (eventual changes in cloud cover) or changes in sun exposure behaviours (e.g. exposure patterns, clothing). Further tailored data extraction and analysis will be necessary to exploit this climatology in a wide range of environmental, occupational and public health applications.

Funding

Part of this work was supported by the Swiss National Science Foundation (SNF) grant CR23I3_152803

CRediT authorship contribution statement

Laurent Vuilleumier: Conceptualization, Methodology, Software, Investigation, Writing - review & editing. **Todd Harris:** Software, Investigation, Writing - review & editing. **Athanasios Nenes:** Writing - review & editing. **Claudine Backes:** Writing - review & editing. **David Vernez:** Conceptualization, Methodology, Writing - original draft.

Declaration of Competing Interest

The authors declare that they have no known competing financial interests or personal relationships that could have appeared to influence the work reported in this paper.

Appendix

Similarly to Fig. 5, Fig. A1 shows for every pixel the average *clear-sky* UV daily dose on a flat horizontal surface expressed in standard erythemal dose (SED). In this case, the estimation for clear-sky irradiance is used to compute the UV daily dose integrated over 24 h for each pixel and each day of the 15-year climatology. In the second step, these clear-sky daily doses are used to compute the temporal average over all days in the climatology each pixel. When comparing to Fig. 5, the average daily doses are about 5 to 9 SED higher (Fig. A2) if the cloud effect is not accounted for, and the cloud effect is generally lower in regions known for a fair weather climate. In Fig. A1, the spatial variability is related to the elevation because of the thinner atmospheric layer traversed by UV radiation and the higher surface albedo in mountains (presence of snow).

[1] Meteosat being a geostationary satellite staying above the Equator, regions at high latitude (North and South) are not very well covered due to the viewing angle. Results are not optimal above 60°.

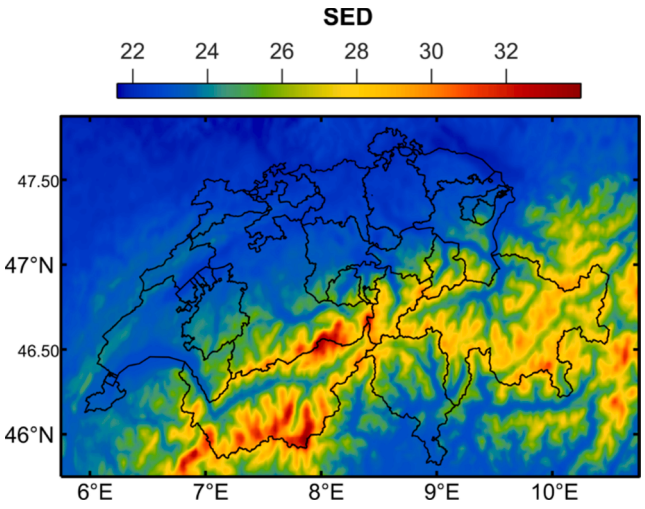

Fig. A1. Map of average clear-sky UV erythemal daily doses (SED) across Switzerland. UV daily doses (24 h exposure) are computed for every pixel and every day of the 15-year climatology and a temporal average over all days is computed for each pixel. The map of Switzerland is given on a longitude, latitude grid.

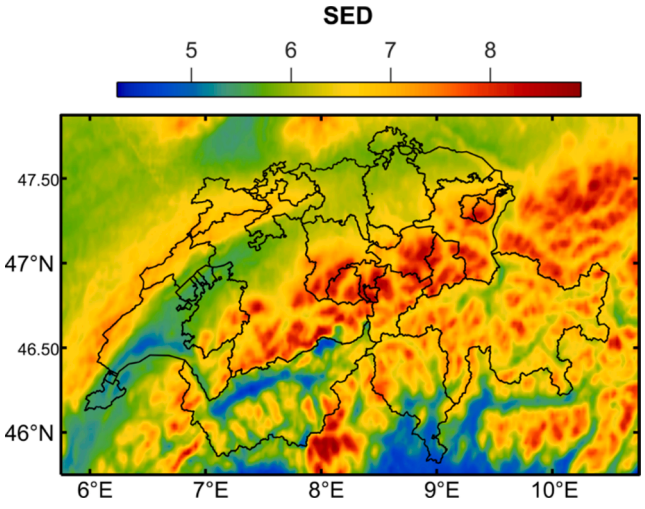

Fig. A2. Map of differences between clear-sky and all-sky UV erythemal daily doses (SED) across Switzerland. For both clear-sky and all-sky, UV daily doses (24 h exposure) are computed for every pixel and every day of the 15-year climatology and a temporal average over all days is computed for each pixel. The map of Switzerland is given on a longitude, latitude grid.

References

Armstrong, B.K., Kricker, A., 2001. The epidemiology of UV induced skin cancer. J Photochem Photobiol B 63, 8–18. https://doi.org/10.1016/S1011-1344(01)00198-1.

Backes, C., Religi, A., Moccozet, L., Vuilleumier, L., Vernez, D., Bulliard, J.L., 2018. Facial exposure to ultraviolet radiation: Predicted sun protection effectiveness of various hat styles. Photodermatol Photoimmunol Photomed 34, 330–337. https://doi.org/10.1111/phpp.12388.

Bernhard, G., Seckmeyer, G., 1999. Uncertainty of measurements of spectral solar UV irradiance. J Geophys Res 104 (D12), 14321–14345. https://doi.org/10.1029/1999JD900180.

Bilbao, J., Román, R., De Miguel, A., Mateos, D., 2011. Long-term solar erythemal UV irradiance data reconstruction in spain using a semiempirical method. J. Geophys. Res. 116, D22211. https://doi.org/10.1029/2011JD015836.

Bodeker, G.E., McKenzie, R.L., 1996. An algorithm for inferring surface UV irradiance including cloud effects. J Appl Meteor 35, 1860–1877. https://doi.org/10.1175/1520-0450(1996)035<1860:AAFISU>2.0.CO;2.

Cano, D., Monget, J.M., Albuisson, M., Guillard, H., Regas, N., Wald, L., 1986. A method for the determination of the global solar radiation from meteorological satellite data. Sol Energy 37, 31–39. https://doi.org/10.1016/0038-092X(86)90104-0.

Cantorna, M.T., 2006. Vitamin D and its role in immunology: Multiple sclerosis, and inflammatory bowel disease. Prog Biophys Mol Biol 92, 60–64. https://doi.org/10.1016/j.pbiomolbio.2006.02.020.

Deluca, H.F., 2014. History of the discovery of vitamin D and its active metabolites. Bonekey Rep 3, 479. https://doi.org/10.1038/bonekey.2013.213.

den Outer, P.N., Slaper, H., Tax, R.B., 2005. UV radiation in the netherlands: Assessing long-term variability and trends in relation to ozone and clouds. J Geophys Res 110, D02203. https://doi.org/10.1029/2004JD004824.

den Outer, P.N., Slaper, H., Kaurola, J., Lindfors, A., Kazantzidis, A., Bais, A.F., et al., 2010. Reconstructing of erythemal ultraviolet radiation levels in europe for the past 4 decades. J Geophys Res 115, D10102. https://doi.org/10.1029/2009JD012827.

Gies, P., van Deventer, E., Green, A.C., Sinclair, C., Tinker, R., 2018. Review of the global solar UV index 2015 workshop report. Health Phys 114, 84–90. https://doi.org/10.1097/HP.0000000000000742.

Hulsen, G., Grobner, J., 2007. Characterization and calibration of ultraviolet broadband radiometers measuring erythemally weighted irradiance. Appl Opt 46 (23), 5877–5886. https://doi.org/10.1364/AO.46.005877.

Kaurola, J., Lindfors, A., Lakkala, K., Hansen, G., Josefsson, W., Vuilleumier, L., et al., 2010. On the usability of the ERA-40 reanalysis in the estimation of past surface UV radiation over europe. J Geophys Res 115, D24107. https://doi.org/10.1029/2010JD013810.

Koepke, P., Backer, H.D., Bais, A., Curylo, A., Eerme, K., Feister, U., et al., 2006. Modelling solar UV radiation in the past: Comparison of algorithms and input data. In: Slusser, J.R., Schäfer, K., Comerón, A. (Eds.). Remote sensing of clouds and the atmosphere, vl XI, 636215 doi:10.1117/12.687682.

Lindfors, A., Vuilleumier, L., 2005. Erythemal UV at Davos (Switzerland), 1926–2003, estimated using total ozone, sunshine duration, and snow depth. J Geophys Res 110, D02104. https://doi.org/10.1029/2004JD005231.

Long, C.N., Ackerman, T.P., 2000. Identification of clear skies from broadband pyranometer measurements and calculation of downwelling shortwave cloud effects. J Geophys Res 105 (D12), 15609–15626. https://doi.org/10.1029/2000JD900077.

Lucas, R.M., McMichael, A.J., Armstrong, B.K., Smith, W.T., 2008. Estimating the global disease burden due to ultraviolet radiation exposure. Int J Epidemiol 37 (3), 654–667. https://doi.org/10.1093/ije/dyn017.

Martineau, A.R., Jolliffe, D.A., Greenberg, L., Aloia, J.F., Bergman, P., Dubnov-Raz, G., et al., 2019. Vitamin D supplementation to prevent acute respiratory infections: Individual participant data meta-analysis. Health Technol Asses 23 (2), 1–44. https://doi.org/10.3310/hta23020.

Mayer, B., Kylling, A., 2005. Technical note: The libRadtran software package for radiative transfer calculations - description and examples of use. Atmos Chem Phys 5, 1855–1877. https://doi.org/10.5194/acp-5-1855-2005.

McKinlay, A.F., Diffey, B.L., 1987. A reference action spectrum for ultra-violet induced erythema in human skin. In: Passchier, W.F., Bosnjakovich, B.F.M. (Eds.), Human exposure to ultraviolet radiation: Risks and regulations. Elsevier Science Ltd, pp. 83–87.

Milon, A., Bulliard, J.L., Vuilleumier, L., Danuser, B., Vernez, D., 2014. Estimating the contribution of occupational solar ultraviolet exposure to skin cancer. Br J Dermatol 170, 157–164. https://doi.org/10.1111/bjd.12604.

Modenese, A., Ruggieri, F.P., Bisegna, F., Borra, M., Burattini, C., Della Vecchia, E., et al., 2019. Occupational exposure to solar UV radiation of a group of fishermen working in the Italian North Adriatic sea. Int J Environ Res Public Health 16, 3001. https://doi.org/10.3390/ijerph16163001.

Moldovan, H.R., Wittlich, M., John, S.M., Brans, R., Tiplica, G.S., Salavastru, C., et al., 2019. Exposure to solar UV radiation in outdoor construction workers using personal dosimetry. Environ Res 181, 108967. https://doi.org/10.1016/j.envres.2019.108967.

Möser, W., Raschke, E., 1984. Incident solar radiation over Europe estimated from Meteosat data. J Climate Appl Meteor 23, 166–170. https://doi.org/10.1175/1520-0450(1984)023<0166:ISROEE>2.0.CO;2.

Mueller, R.W., Dagestad, K.F., Ineichen, P., Schroedter-Homscheidt, M., Cros, S., Dumortier, D., et al., 2004. Rethinking satellite-based solar irradiance modelling: The SOLIS clear-sky module. Remote Sens Environ 91, 160–174. https://doi.org/10.1016/j.rse.2004.02.009.

Ohmura, A., Dutton, E.G., Forgan, B., Fröhlich, C., Gilgen, H., Hegner, H., et al., 1998. Baseline Surface Radiation Network (BSRN/WCRP): new precision radiometry for climate research. Bull Amer Meteor Soc 79, 2115–2136. doi:10.1175/1520-0477(1998)079<2115:BSRNBW>2.0.CO;2.

Posselt, R., Mueller, R.W., Stöckli, R., Trentmann, J., 2012. Remote sensing of solar surface radiation for climate monitoring — the CM-SAF retrieval in international comparison. Remote Sens Environ 118, 186–198. https://doi.org/10.1016/j.rse.2011.11.016.

Posselt, R., Mueller, R., Trentmann, J., Stockli, R., Liniger, M.A., 2014. A surface radiation climatology across two Meteosat satellite generations. Remote Sens Environ 142, 103–110. https://doi.org/10.1016/j.rse.2013.11.007.

Religi, A., Backes, C., Chatelan, A., Bulliard, J.L., Vuilleumier, L., Moccozet, L., et al., 2019. Estimation of exposure durations for vitamin D production and sunburn risk in Switzerland. J Expo Sci Environ Epidemiol 29, 742–752. https://doi.org/10.1038/s41370-019-0137-2.

Stöckli, R., 2013. The HelioMont surface solar radiation processing (2017 update). Scientific report MeteoSwiss, 93. Federal Office of Meteorology and Climatology MeteoSwiss, Zurich, Switzerland.

van Weele, M., van der A, R.J., van Geffen, J., Roebeling, R. 2005. Space-based surface UV monitoring for Europe using SCIAMACHY and MSG. In: Proc. SPIE 5979, Remote Sensing of Clouds and the Atmosphere X. doi:10.1117/12.626516.

Vernez, D., Milon, A., Francioli, L., Bulliard, J.-L., Vuilleumier, L., Moccozet, L., 2011. A numeric model to simulate solar individual ultraviolet exposure. Photochem Photobiol 87, 721–728. https://doi.org/10.1111/j.1751-1097.2011.00895.x.

Vernez, D., Milon, A., Vuilleumier, L., Bulliard, J.-L., Koechlin, A., Boniol, M., et al., 2015. A general model to predict individual exposure to solar UV by using ambient irradiance data. J Expo Sci Environ Epidemiol 25, 113–118. https://doi.org/10.1038/jes.2014.6.

Vienneau, D., de Hoogh, K., Hauri, D., Vicedo-Cabrera, A.M., Schindler, C., Huss, A., et al., 2017. Effects of radon and UV exposure on skin cancer mortality in Switzerland. Environ Health Perspect 125 (6), 067009. https://doi.org/10.1289/EHP825.

Vuilleumier, L., Meyer, A., Stöckli, R., Wilbert, S., Zarzalejo, L.F., 2020. Accuracy of satellite-derived solar direct irradiance in Southern Spain and Switzerland. Int J Remote Sens 41, 8808–8838. https://doi.org/10.1080/01431161.2020.1783712.

Wald, L., 2012. https://hal-mines-paristech.archives-ouvertes.fr/hal-00788420.